

Article

## Electromagnetic Analysis and Design of Switched Reluctance Double-Rotor Machine for Hybrid Electric Vehicles

Shouliang Han, Shumei Cui \*, Liwei Song and Ching Chuen Chan

Department of Electrical Engineering, Harbin Institute of Technology, Harbin 150080, China;  
E-Mails: andyhan@hit.edu.cn (S.H.); song\_lw@hit.edu.cn (L.S.); ccchan@eee.hku.hk (C.C.C.)

\* Author to whom correspondence should be addressed; E-Mail: cuism@hit.edu.cn;  
Tel./Fax: +86-451-8640-2089.

External Editor: Susan Krumdieck

Received: 1 July 2014; in revised form: 11 September 2014 / Accepted: 29 September 2014 /  
Published: 16 October 2014

---

**Abstract:** The double-rotor machine is a kind of multiple input and output electromechanical energy transducer with two electrical ports and two mechanical ports, which is an ideal transmission system for hybrid electric vehicles and has a series of advantages such as integration of power and energy, high efficiency and compaction. In this paper, a switched reluctance double-rotor machine (SRDRM) is proposed for hybrid electric vehicles, while no conductor or PM in the middle rotor. This machine not only inherits the merits of switched reluctance machine, such as simple salient rotor structure, high reliability and wide speed range, but also can avoid the outer rotor's cooling problem effectively. By using an equivalent magnetic circuit model, the function of middle rotor yoke is analyzed. Electromagnetic analyses of the SRDRM are performed with analytical calculations and 2-D finite element methods, including the effects of main parameters on performance. Finally, a 4.4 kW prototype machine is designed and manufactured, and the tests are performed, which validate the proposed design method.

**Keywords:** switched reluctance double-rotor machine (SRDRM); electromagnetic analysis; equivalent magnetic circuit model; hybrid electric vehicles

---

## 1. Introduction

Double Rotor Machine (DRM) is an electro-mechanical energy converter based on the traditional single rotor machine by increasing the number of rotors. There are two mechanical ports and two electrical ports, which allow the energy transformed between these four ports bidirectionally. When applied in Hybrid Electrical Vehicle (HEV), the DRM can achieve different functionalities such as motoring, generating, as well as continuous variable transmission. The electrical and mechanical energy can be adjusted accordingly to achieve high efficiency and dynamic performance. The clutches, gear transmission and alternator can be replaced by the DSM, which is a novel vehicle transmission system [1–3].

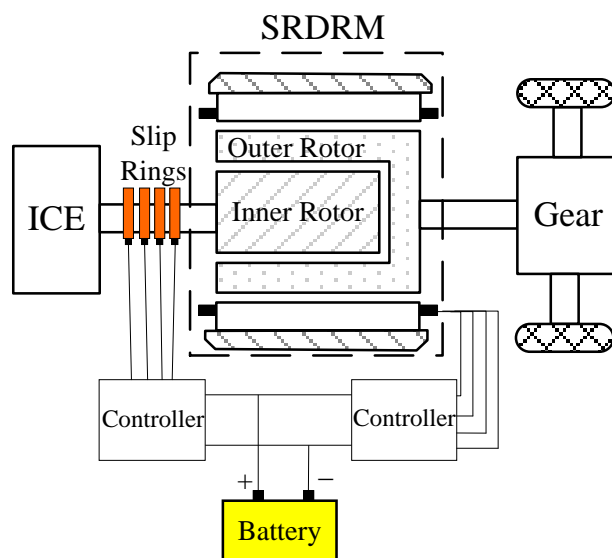
At present, researches of induction machine (IM) [4] and permanent magnet (PM) [5] based on DRM have been very common. Many researchers are working to solve the problems of field coupling control strategy [6], cooling of the inner rotor [7], manufacture and totally brushless configurations [8]. They set a foundation for practical application. However, there are a lot of problems to be further studied.

Some scholars have started to study the switched reluctance based on DRM (SRDRM) [9]. Both theoretical analysis and experimental results show that SRDRM not only has the same advantages as PMDRM but also can be operated in different modes flexibly, which makes SRDRM an interesting candidate for HEVs [10].

By employing switched reluctance machine, SRDRM can be established, which inherits the merits of switched reluctance machine [11]: (1) Simple structure without conductors or PMs on the rotor; (2) concentrated windings with short end on the stator without phase jumper wire, which offers high reliability; (3) wide constant power speed range, which is suitable for traction application.

The scheme of SRDRM drivetrain in a hybrid system is shown in Figure 1. It offers flexible speed and torque transmission, which allows the engine to operate in the efficient optimized region under different working conditions. Thus, fuel economy and emission performances can be significantly improved.

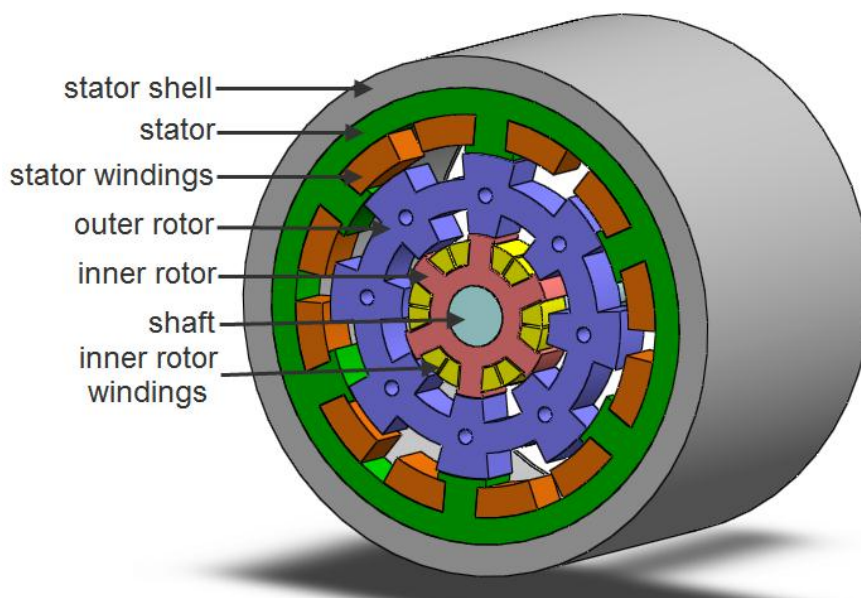
**Figure 1.** SRDRM in hybrid electric vehicle system.



In this paper, a kind of SRDRM is proposed for hybrid electric vehicles. It integrates two switched reluctance machines, *i.e.*, an outer motor which consists of the stator and the outer rotor and an inner

motor which consists of the outer rotor and the inner rotor, with two independent mechanical output shafts. The armature windings are located in the stator and inner rotor, and there are no conductors or PMs in the outer rotor, showing in Figure 2. Compared to other DRMs, SRDRM not only has the advantage of rigid rotor structure, high reliability and wide speed range, but also gets rid of the cooling problem of the outer rotor. As shown in the Figure 2, the SRDRM is composed of two switched reluctance machines which share one solid rotor. Both the stator and inner rotor windings are connected to batteries through DC/AC inverters respectively.

**Figure 2.** Structure of SRDRM.



By using an equivalent magnetic circuit model, the function of the outer rotor yoke is analyzed. Electromagnetic analyses of the SRDRM are performed with analytical calculations and 2-D finite element methods, including the effects of main parameters on performance. Finally, a 4.4 kW prototype machine is designed and manufactured, and the experimental tests are done to validate the proposed design.

## 2. Magnetic Equivalent Circuit Analysis of SRDRM

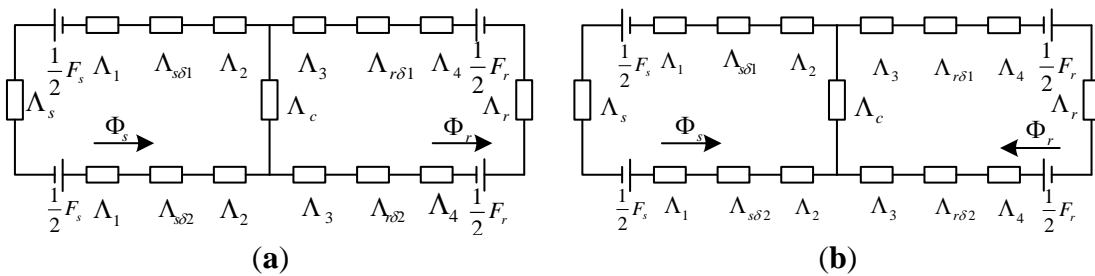
Based upon equivalent magnetic flux principle, the magnetic model can be established. The magnetic circuit model describes the magneto-motive force (MMF), flux and flux paths in the machine as different components in an electrical circuit [12], in which the detailed analysis of the magnetic distribution is not necessary. The equivalent magnetic circuit model follows the magnetic Ohm's law and magnetic Kirchhoff's law, and the following relationship is established:

$$U_i = R_i \Phi_i, \sum_1^n U_i = \sum_1^m F_i, \sum_1^m \Phi_i = 0 \quad (1)$$

where,  $U_i$  is the magnetic voltage drop;  $R_i$  is the magnetic reluctance;  $\Phi_i$  is the magnetic flux flow;  $F_i$  is the MMF of the branch;  $n$  is the node number of the magnetic model;  $m$  is the branch number of each node.

In order to establish the SRDRM equivalent model, the edge effects and magnetic flux non-linearity are neglected and the magnetic steel permeability is considered to be infinity  $\mu = \infty$ . When the stator and inner rotor are energized at the same time, the equivalent magnetic circuit models of SRDRM are shown in Figure 3.

**Figure 3.** Equivalent magnetic circuits of SRDRM: (a) MMF directions of stator and rotor windings are the same; (b) MMF directions of stator and rotor windings are opposite.



Where  $F_s$ ,  $F_r$  are the stator and inner rotor MMF established by the excited armature windings respectively;  $\Lambda_s$ ,  $\Lambda_c$  and  $\Lambda_r$  are the permeances of stator yoke, outer rotor yoke and inner rotor yoke respectively;  $\Lambda_{s\delta 1}$  and  $\Lambda_{s\delta 2}$  are the air gap permeances under stator poles;  $\Lambda_{r\delta 1}$  and  $\Lambda_{r\delta 2}$  are the air gap permeances under inner rotor poles;  $\Lambda_1$ ,  $\Lambda_2$ ,  $\Lambda_3$  and  $\Lambda_4$  are the permeances of stator tooth, outer rotor's outer tooth, outer rotor's inner tooth and inner rotor tooth respectively.

When the current is low, the permeances of stator, outer rotor, and inner rotor are all constants, while the double salient structure changes the gap permeance with the variations of outer rotor's position angle, namely:

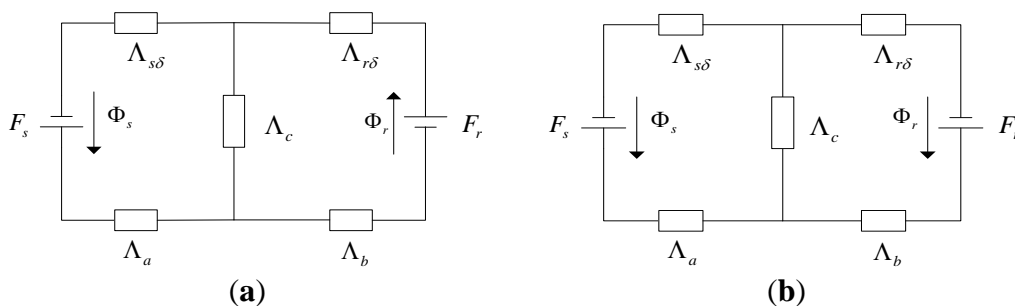
$$\Lambda_{\delta} = \Lambda_{\delta}(\theta) \tag{2}$$

Define

$$\begin{cases} \Lambda_a = \Lambda_s + 2\Lambda_1 + 2\Lambda_2 \\ \Lambda_{s\delta} = \Lambda_{s\delta 1} + \Lambda_{s\delta 2} \\ \Lambda_b = \Lambda_r + 2\Lambda_3 + 2\Lambda_4 \\ \Lambda_{r\delta} = \Lambda_{r\delta 1} + \Lambda_{r\delta 2} \end{cases} \tag{3}$$

The magnetic circuit in Figure 3 can be simplified as Figure 4:

**Figure 4.** Simplified equivalent magnetic circuits diagrams of SRDRM: (a) MMF directions of stator and rotor windings are the same; (b) MMF directions of stator and rotor windings are opposite.



Apply the Kirchoff's loop law on Figure 4a, the mathematical equations are obtained:

$$\begin{cases} \Phi_s \left( \frac{1}{\Lambda_{s\delta}} + \frac{1}{\Lambda_a} + \frac{1}{\Lambda_c} \right) - \Phi_r \frac{1}{\Lambda_c} = F_s = N_s I_s \\ \Phi_r \left( \frac{1}{\Lambda_{r\delta}} + \frac{1}{\Lambda_b} + \frac{1}{\Lambda_c} \right) - \Phi_s \frac{1}{\Lambda_c} = F_r = N_r I_r \end{cases} \quad (4)$$

Solving the equations:

$$\begin{cases} \Phi_s = \frac{R_2 N_s I_s + R_c N_r I_r}{R_1 R_2 - R_c^2} \\ \Phi_r = \frac{R_c N_s I_s + R_1 N_r I_r}{R_1 R_2 - R_c^2} \end{cases} \quad (5)$$

where,

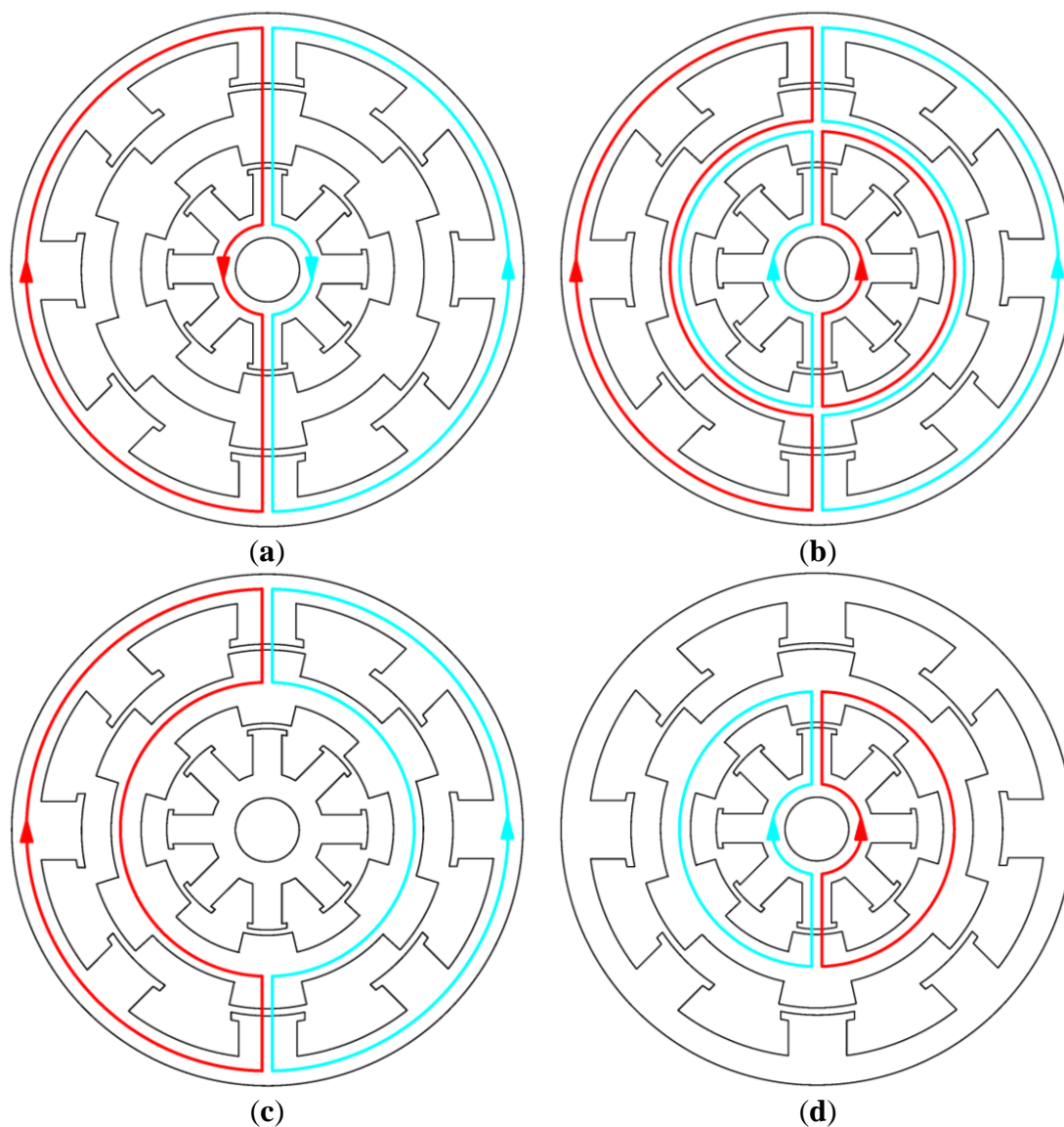
$$\begin{cases} \frac{1}{\Lambda_{s\delta}} + \frac{1}{\Lambda_a} + \frac{1}{\Lambda_c} = R_1 \\ \frac{1}{\Lambda_{r\delta}} + \frac{1}{\Lambda_b} + \frac{1}{\Lambda_c} = R_2 \\ \frac{1}{\Lambda_c} = R_c \end{cases} \quad (6)$$

From the equations above, the magnetic flux of stator and inner rotor is related to both excitations of the stator and the inner rotor. When the stator and rotor excitations satisfy certain relationship,  $\Phi_s = \Phi_r$ , there is no magnetic line of force in the outer rotor's yoke, as can be seen in Figure 5a. Therefore, the outer rotor's yoke can be designed very thin. When the excitation works in the opposite directions, both flux lines from stator and inner rotor travel in the outer rotor yoke, as shown in Figure 5b. In this case, the outer rotor's yoke has to be designed very thick; otherwise it will be highly saturated. And the output torque will be affected significantly. When the stator winding is energized alone, the majority of the magnetic flux lines travel through the outer rotor yoke, because the outer rotor's yoke reluctance  $R_c$  is much smaller than  $R_2$ . The magnetic flux enters into the inner rotor core only when the outer rotor's yoke is highly saturated, as shown in Figure 5c. Figure 5d shows the magnetic flux line distribution when the inner rotor winding is energized alone. Four cases may occur when SRDRM runs, so the outer rotor's yoke should be sized for the heaviest magnetic condition.

When the machine geometry parameters are determined,  $R_c$  in Equation (6) is fixed, and  $R_1$  and  $R_2$  are two groups of magnetization curves of the outer rotor angular position. The phase current and magnetic energy storage can be obtained by calculating the flux linkage and its variation, such that the transient electromagnetic torque can be derived.

From the analysis above, it can also be seen that the outer rotor's magnetic yoke is very important in the electromagnetic design of SRDRM. Small  $R_c$  results in small electromagnetic interference between the inner and outer motor. Increasing the thickness of the outer rotor can reduce  $R_c$ , however, a thicker outer rotor leads to a bigger diameter of stator, which will significantly increase the size and weight of the machine.

**Figure 5.** Different magnetic circuits of SRDRM: (a) Magnetic circuit in series; (b) Magnetic circuit in parallel; (c) Stator winding works alone; (d) Inner rotor winding works alone.



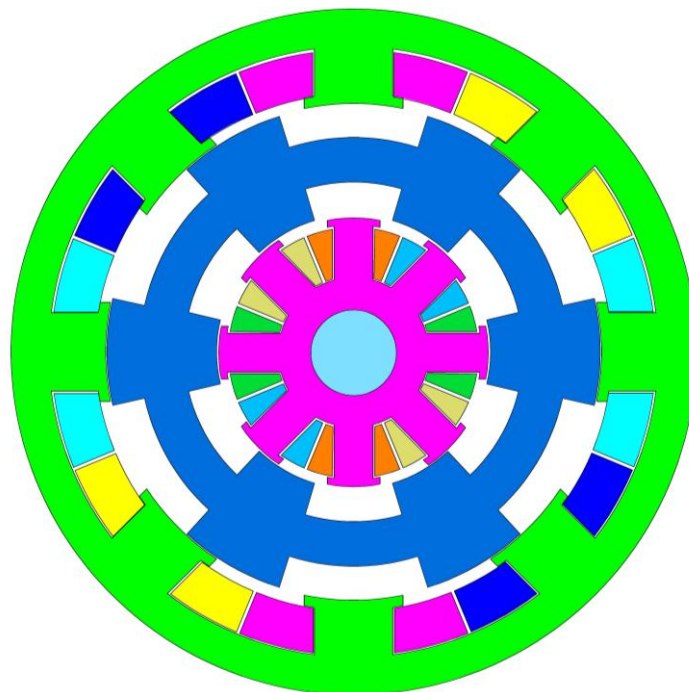
### 3. Finite Element Analysis of SRDRM

Due to the high saturation of the motor, magnetizing characteristics ( $\Psi$ - $i$ ) of SRM have to be calculated under different excitations and different rotor positions. Finite element analysis (FEA), one of the most effective tools for electromagnetic analysis, is utilized in this paper by Maxwell 2D software. The transient performance of each motor in the SRDRM is analyzed individually by injecting current to one of the motor windings. Effects of magnetic coupling between these two motors on the SRDRM performance are simulated under static state.

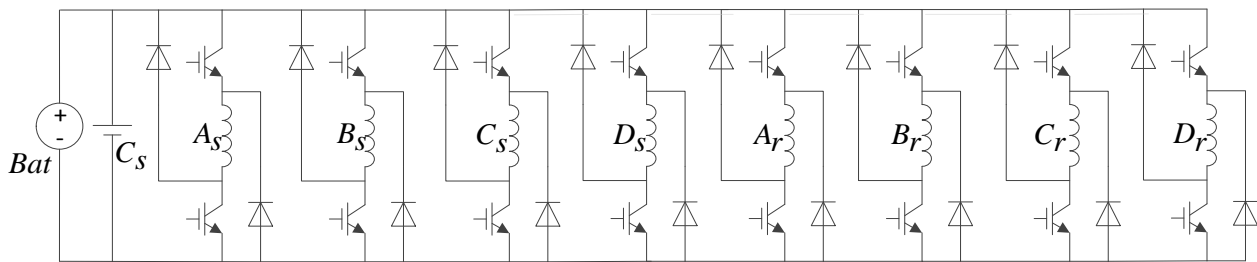
In order to simplify the design and FEA, performance indexes of inner motor and outer motor are the same, including voltage, rated speed and rated power. The internal and external armature winding are fed by two controllers independently. The key design data are listed in Table 1. Figure 6 shows the 2D FEA model of SRDRM.

**Table 1.** Main parameters of the SRDRM.

Parameters	Outer Motor	Inner Motor
Rated RMS Voltage (V)	380	380
Rated Power (kW)	2.2	2.2
Maximum Power (kW)	4.4	2.2
Number of Phases	4	4
Number of poles	8/6	8/6
Rated Speed (rpm)	1500	1500
Maximum Speed (rpm)	3000	3000
Air Gap (mm)	0.4	0.4
Outer Diameter of Stator (mm)	200	-
Outer Diameter of Outer Rotor (mm)	144	-
Outer Diameter of Inner Rotor (mm)	-	79.2
Diameter of Shaft (mm)	-	20
Stator/Inner Rotor Pole Arc (°)	23	23
Outer Rotor Pole Arc (°)	27	27
Length of Core (mm)	130	130
Number of Turns for one phase	84	74

**Figure 6.** 2D FEA model of SRDRM.

The control method is angular position control (APC), which is to control both the outer rotor and inner rotor by adjusting the turn-off and turn-on angles to obtain large current, high motoring torque, and low copper loss [13]. The main power circuit is as shown in Figure 7.

**Figure 7.** The main power circuit of SRDRM.

### 3.1. Machine Performances only the Stator Winding is Excited

When only the stator winding is excited, the flux line distributions of the SRDRM are shown in Figure 8, with respect to the unaligned and aligned position. The flux route can be divided into 3 parts: the main flux which links the stator poles, rotor poles and air gap; the leakage flux which travels from the excited stator pole directly to the stator yoke through the gap between poles; and the leakage flux travels from the excited stator pole to the adjacent stator poles. Figure 9 shows the space flux density with respect to different operating condition. When the stator windings are excited, the outer motor air gap flux density varies with the exciting sequence. The peak flux density occurs when the rotor and stator poles are about to detach. There is no flux line travels into the inner rotor, which reflects that the inner rotor doesn't affect the operation of the outer motor.

The winding flux-linkage varies with the excitations under different rotor position. Figure 10 shows the magnetizing characteristic of the outer motor from unaligned to aligned position. When the motor is unaligned, the flux-linkage varies linearly with the current. When the rotor pole tends to align with the stator pole, the flux-linkage varies nonlinearly with the current. The flux-linkage increase significantly when the rotor pole is moving towards the stator pole, however, due to the saturation, the flux-linkage increasing rate drops greatly when the rotor pole and stator pole are about to align.

**Figure 8.** Magnetic line distributions: (a) Outer rotor unaligned position; (b) Outer rotor aligned position.

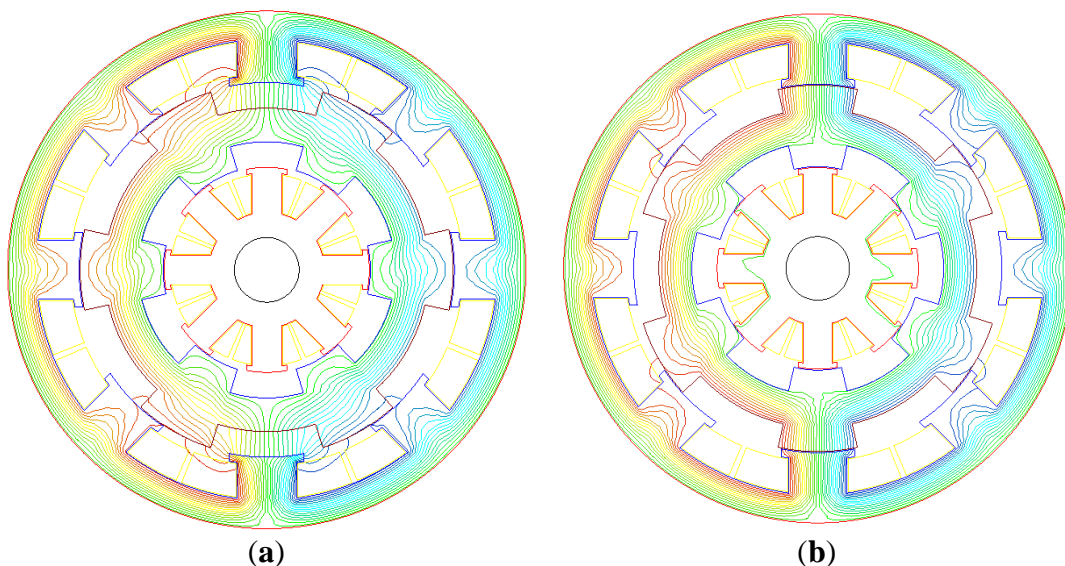


Figure 9. 3-D graph of flux density in the outer air gap.

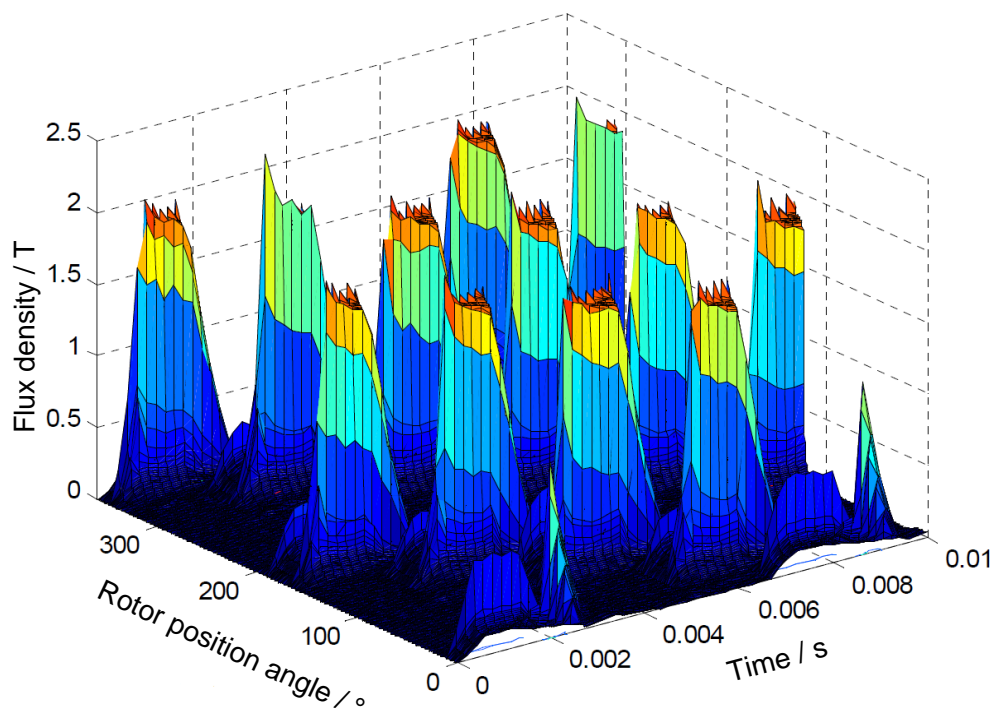
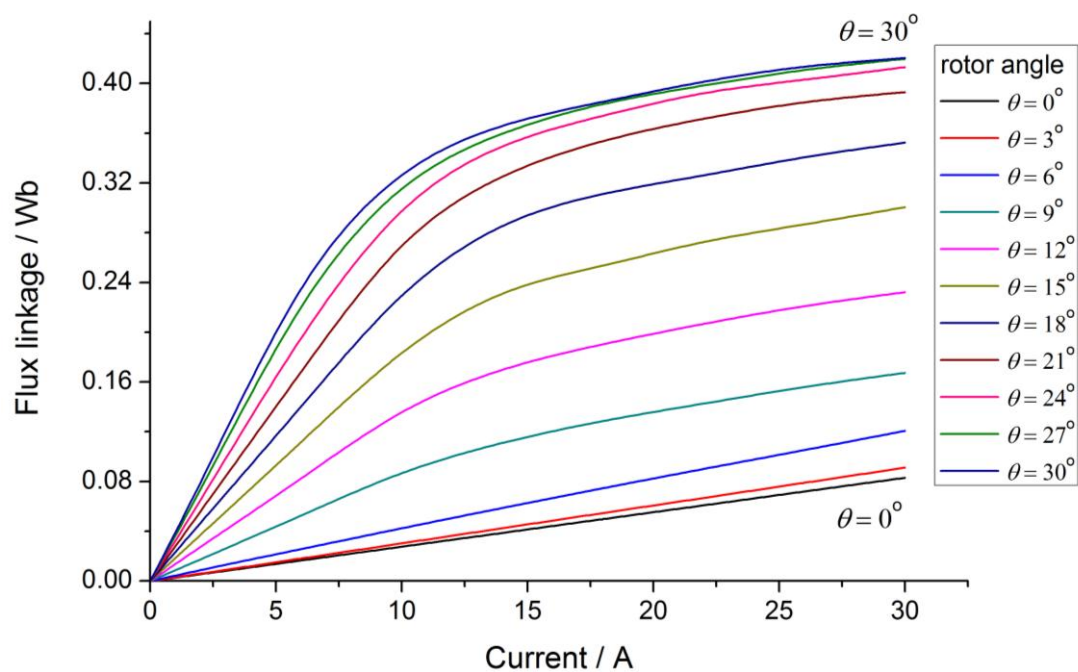


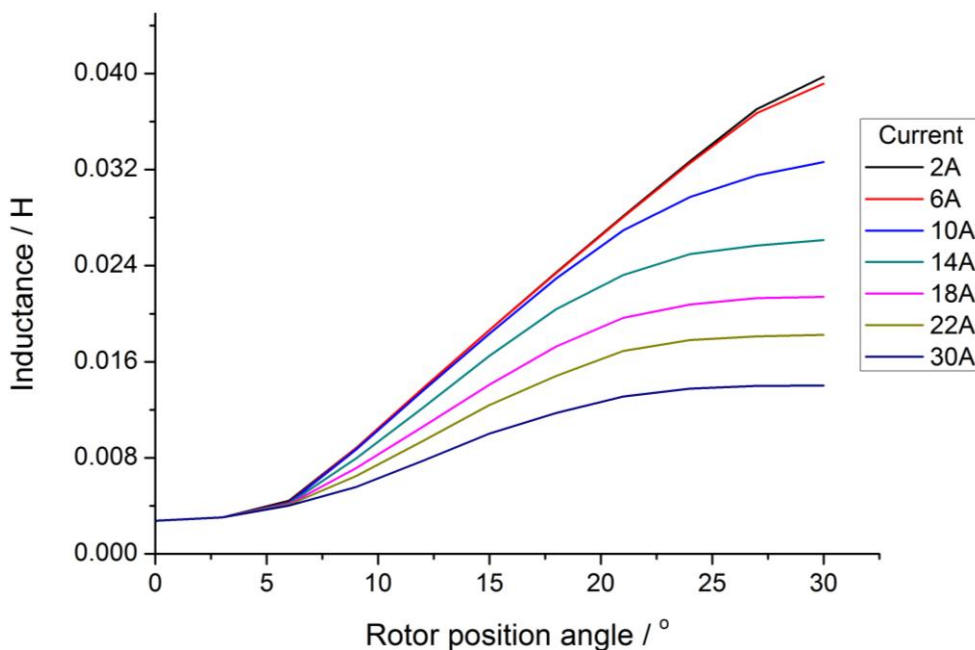
Figure 10. Magnetizing characteristic ( $\Psi$ - $i$ ) curves of one phase.



$$L(\theta, i) = \frac{\psi(\theta, i)}{i} \tag{7}$$

The inductance profile can be derived from flux linkage information by Equation (7). In Figure 11, the inductance curves correspond to different currents respectively, which reveals that the inductance varies significantly with both rotor position  $\theta$  and current.

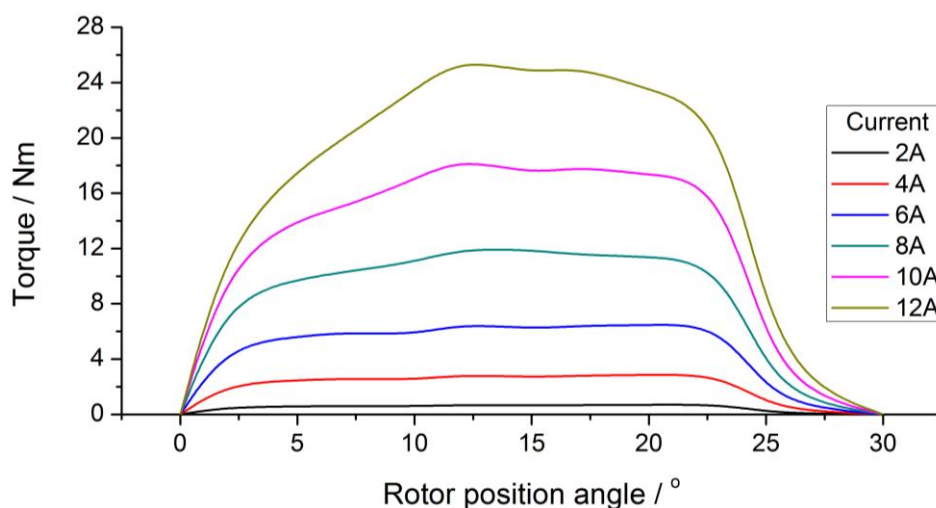
**Figure 11.** Inductance curves of stator winding.



$$\begin{cases} W_m' = \int_0^i \psi(\theta, i) di \\ T = \left. \frac{\partial W_m'}{\partial \theta} \right|_{i=const} \end{cases} \quad (8)$$

The static torque profile can be derived from the partial differential of the co energy, as represented by Equation (8). When one phase of the motor is excited, the static torque varies with not only the current but also the rotor position, see Figure 12.

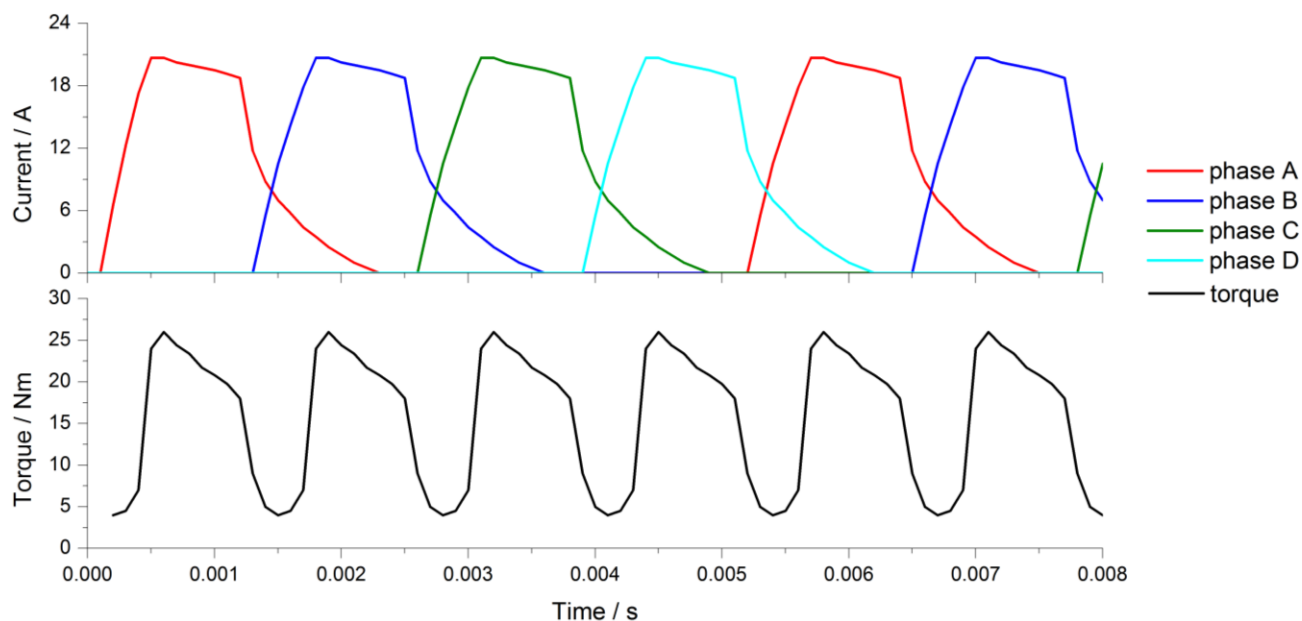
**Figure 12.** Curves of static torque with one phase excited.



When the motor is controlled under single pulse mode,  $\theta_{on} = 0^\circ$ ;  $\theta_{off} = 15^\circ$ , the stator winding current can be divided into three parts: the current rises dramatically due to the small winding inductance when the winding is turned on at unaligned position; the current drops gently due to the high winding inductance when the rotor pole and stator start to overlap; the current drops significantly when the

winding is turned off and the current flows back to the power supply. The current and torque waveform are shown in Figure 13.

**Figure 13.** The current and torque waveforms of outer motor.



### 3.2. Machine Performances only the Inner Rotor Winding Is Excited

Similar to the analysis of the outer motor, the air gap flux density distribution with respect to the spinning of the rotor is shown in Figure 14. When the inner motor is excited, the flux doesn't travel into the stator either.

**Figure 14.** 3-D graph of flux density in the inner air gap.

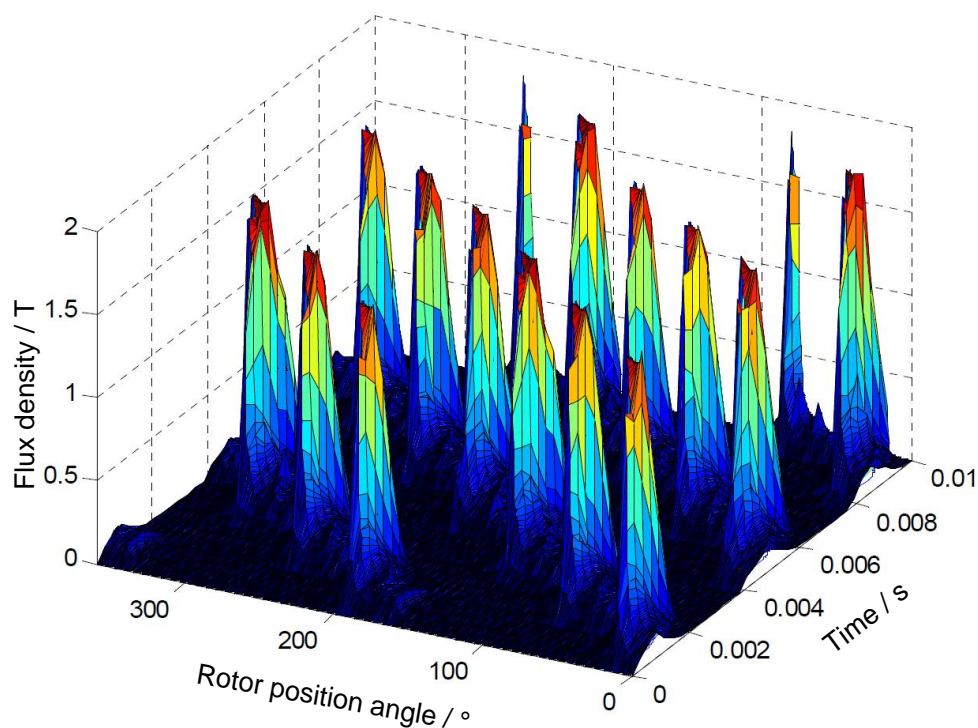
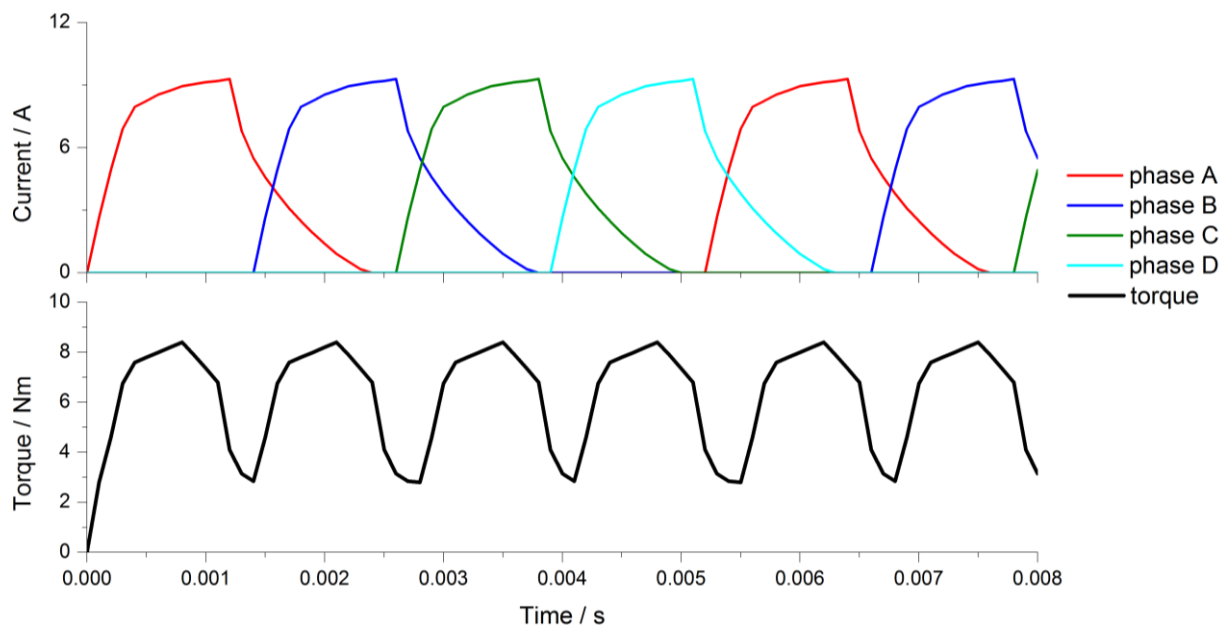


Figure 15 shows the current profile when the inner motor is excited under single pulse control mode and the corresponding synthetic torque waveform.

**Figure 15.** The current and torque waveforms of inner motor.



### 3.3. Machine Performances When Both Stator and Inner Rotor Winding Are Excited

Without considering the transient process, when both stator and inner rotor winding are excited, operation condition of SRDRM is the direction of synthetic torque of inner rotor or outer rotor need to remain static relatively. The case of both inner motor and outer motor running at the electric state is only analyzed in this paper. For the outer motor, speed of the outer rotor and stator magnetic field rotation is synchronous; but for the inner motor, speed of the inner rotor is synthetic speed of two magnetic fields.

The winding configuration of the SRDRM is defined as shown in Figure 16. In order to simplify the analysis, assuming the outer rotor is rotating at 1500 rpm clockwise, the excitation sequence is  $A_1 \rightarrow B_1 \rightarrow C_1 \rightarrow D_1 \rightarrow A_1$  and each phase is conducted for  $15^\circ$  mechanically, *i.e.*,  $60^\circ$  electrical angle. Without considering the inner motor stall condition, the operation of the inner rotor can be in two different situations: outer rotor as the reference, inner rotor rotates clockwise or counterclockwise.

In the simulation, the control strategy adopts angular position control (APC). Supply current is ideal square wave. Stator winding current is 15A, while the inner rotor winding current is 8A.

#### 3.3.1. The Case of Inner Rotor Rotating Clockwise Relatively

Because the frequencies of two controllers are completely independent, the speed of the inner rotor and outer rotor could be independent. Assuming inner rotor runs at 3000 rpm clockwise relative to the stator, the relative speed between the inner rotor and outer rotor is 1500 rpm. In this case, the stator and inner rotor armature windings are fed at a different frequency. The stator excitation sequence would still be  $A_1 \rightarrow B_1 \rightarrow C_1 \rightarrow D_1 \rightarrow A_1$ , but the inner rotor excitation would be  $A_2 \rightarrow D_2 \rightarrow C_2 \rightarrow B_2 \rightarrow A_2$ .

Figure 17 is the flux distribution of the SRDRM of a single moment when both the inner and outer motor are excited. In the different position of the outer rotor core, it has a series magnetic circuit or

a parallel magnetic circuit, which highly depends on the rotor position and the current amplitude. The outer rotor's yoke should be sized for the heaviest magnetic condition. Therefore, the torque performance of each motor is simulated and compared in individual excitation and dual excitation condition.

**Figure 16.** Winding conduction way of SRDRM.

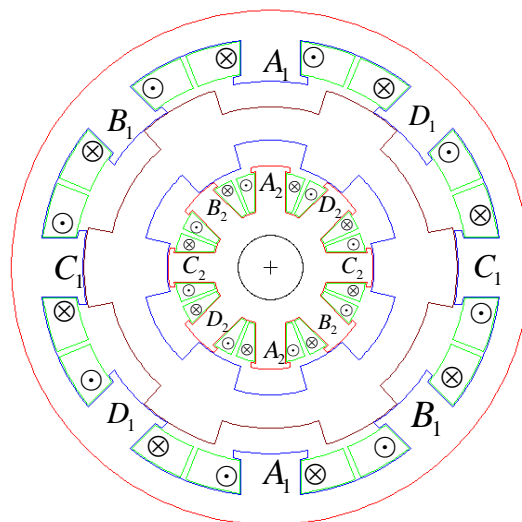


**Figure 17.** Flux distribution of the SRDRM when the inner rotor rotates clockwise relative to the outer rotor.

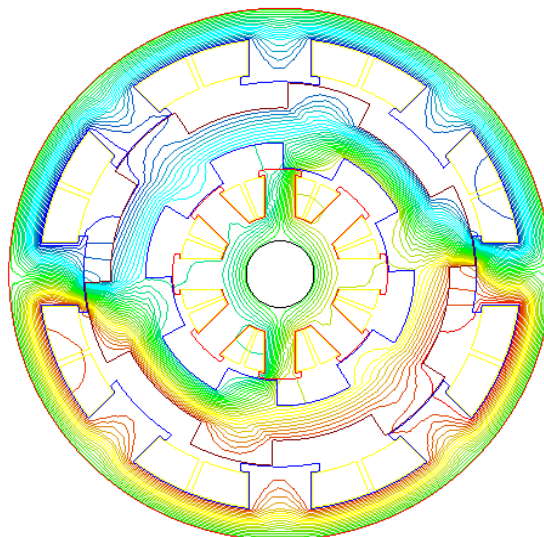


Figure 18 displays the torque performance of the outer motor. The blue curve represents the transient torque when the stator is excited individually and the red curve represents the torque when both the stator and inner rotor armature windings are excited. The average torque is 25 Nm and 13 Nm respectively. Because the inner rotor winding current is about half the stator winding current, the average torque with both the stator and inner rotor armature windings fed is roughly half the average torque with just the stator winding fed. A detailed analysis is given later. The transient torques of these two situations share the similar waveform which means the torque performance of the outer motor is the same under these two situations except for the truth that the inner motor produces a negative torque to reduce the synthetic torque.

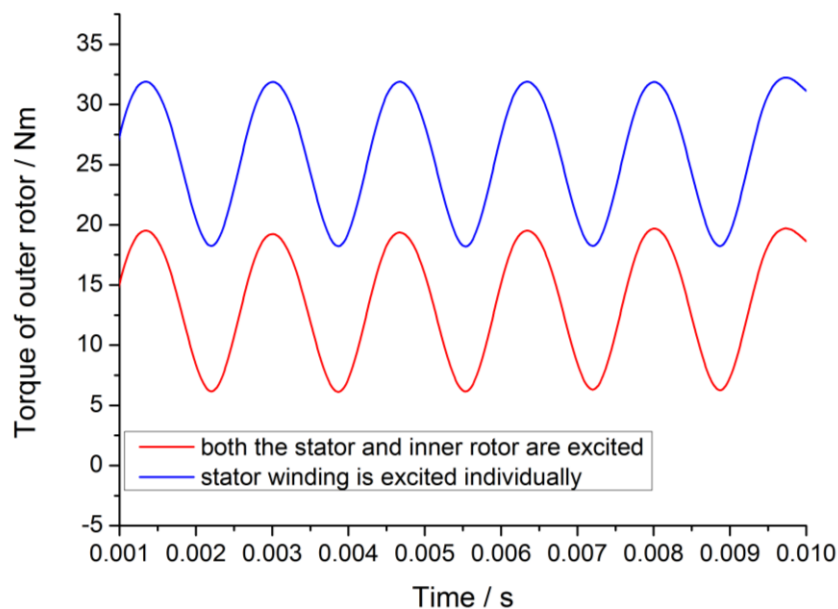
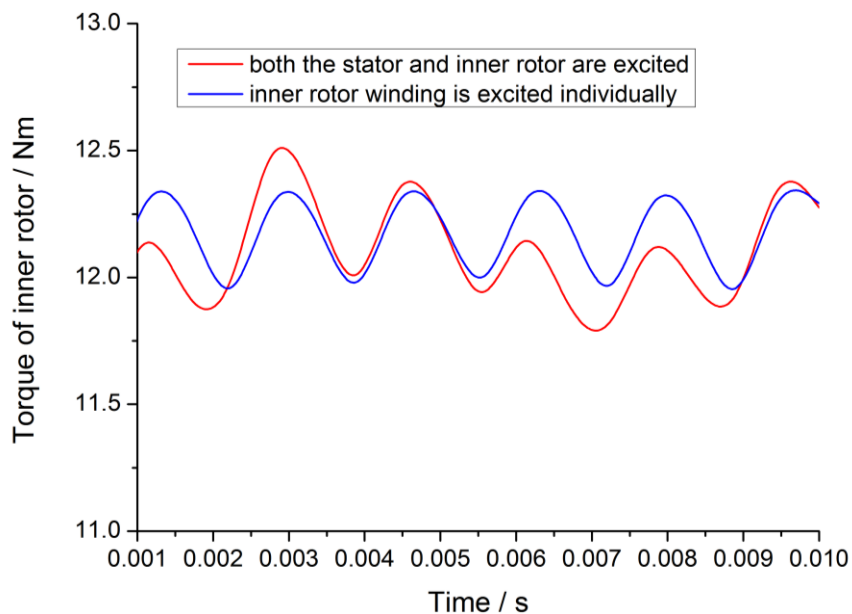
**Figure 18.** The torque waveforms of the outer rotor in different cases.

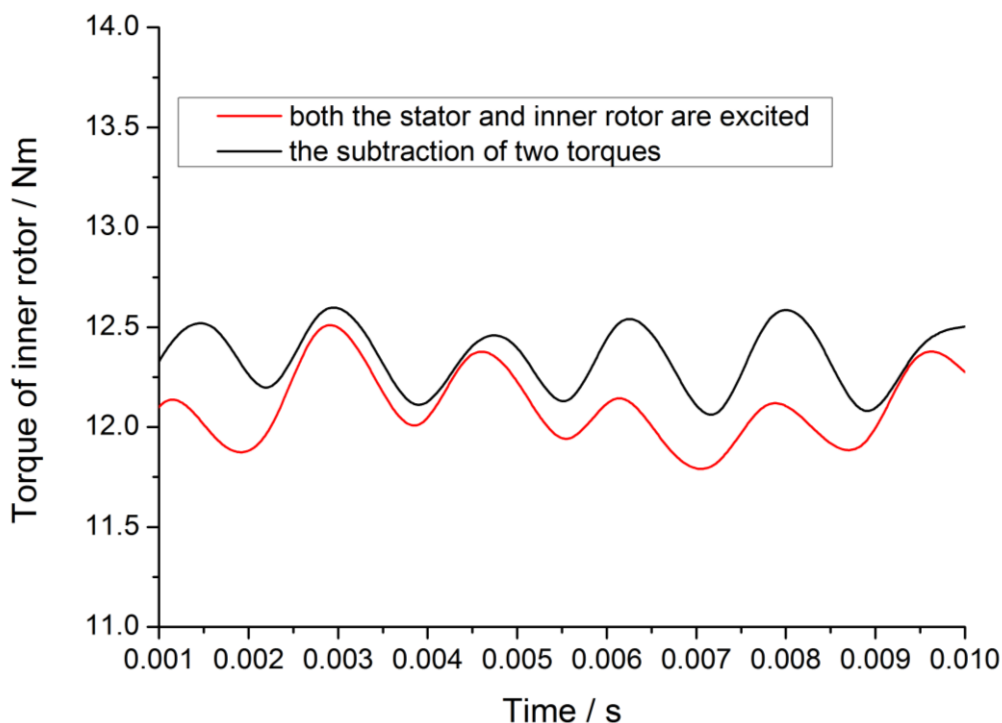
Figure 19 is the torque waveform of the inner rotor under single and dual excitation conditions. The torque waveform matches with each other very well which means that the influence of field coupling on the inner motor torque production can be neglected.

**Figure 19.** The torque waveforms of the inner rotor in different cases.

When the inner rotor spins faster than the outer rotor, the torque waveforms of both the outer and inner rotor are almost the same no matter if the motor is excited in single or dual excitation modes. In order to obtain a clearer understanding of the inner rotor torque, we make a comparison, see Figure 20. The red curve represents the torque of the inner rotor under dual excitation mode, namely, the red curve in Figure 19. The black curve shows the subtraction of outer rotor torque when the stator is excited individually (*i.e.*, blue curve in Figure 18) and the torque when both the stator and inner rotor armature windings are excited (*i.e.*, red curve in Figure 18).

Figure 20 tells that when the inner and outer motor are excited at the same time, the stator winding provides the power to produce the torque of outer motor and inner motor. Part of the torque of the outer rotor is transmitted to the inner rotor. Therefore, the mechanical power is transmitted directly, which brings another advantage of the SRDRM, in other words, the electromechanical conversion system could be much smaller and lighter [1].

**Figure 20.** The torque waveforms comparison of the inner rotor in different cases.



### 3.3.2. The Case of Inner Rotor Rotating Counterclockwise Relatively

When the outer rotor is rotating at 1500 rpm clockwise, assuming the inner rotor runs at 1500 rpm counterclockwise relative to the outer rotor, the relative speed between the inner rotor and the stator is 0 rpm. Then both the inner motor and outer motor rotate at 1500 rpm in a different direction. The excitation sequence of the stator winding and inner rotor winding will be  $A_1 \rightarrow B_1 \rightarrow C_1 \rightarrow D_1 \rightarrow A_1$  and  $A_2 \rightarrow B_2 \rightarrow C_2 \rightarrow D_2 \rightarrow A_2$ , respectively.

Figure 21 is the torque waveform of the outer rotor under single and dual excitation modes. Similar to the situation we discussed above, these two transient torque performances share the similar waveform, but the outer rotor torque under dual excitation is higher than single excitation mode due to the fact that both the inner rotor and stator produce the torque on the outer rotor in the same direction.

Figure 22 shows the torque waveforms of the inner rotor under single and dual excitation modes. When the inner rotor spins slower than the outer rotor, the torque of the inner rotor will decrease due to the effect of field coupling.

The torque of the inner rotor produced from the inner rotor winding can be derived by subtracting the outer rotor torque under single excitation mode from the torque under dual excitation mode, as the black curve shown in Figure 23. As the comparison, the red curve shows the synthetic torque of the inner rotor when both the winding on the stator side and inner rotor side are excited.

From the analysis above, the torque of the outer rotor is the superposition of the torque produced by the outer motor and inner motor and the electrical power from stator winding and inner winding are transferred into the mechanical power of the outer rotor.

Considering the marginal case, when the inner rotor rotates at the same speed as the outer rotor, in which case, the inner motor is in the stall condition, the torque ripple will be more significant and the efficiency drops.

**Figure 21.** The torque waveforms of the outer rotor in different cases.

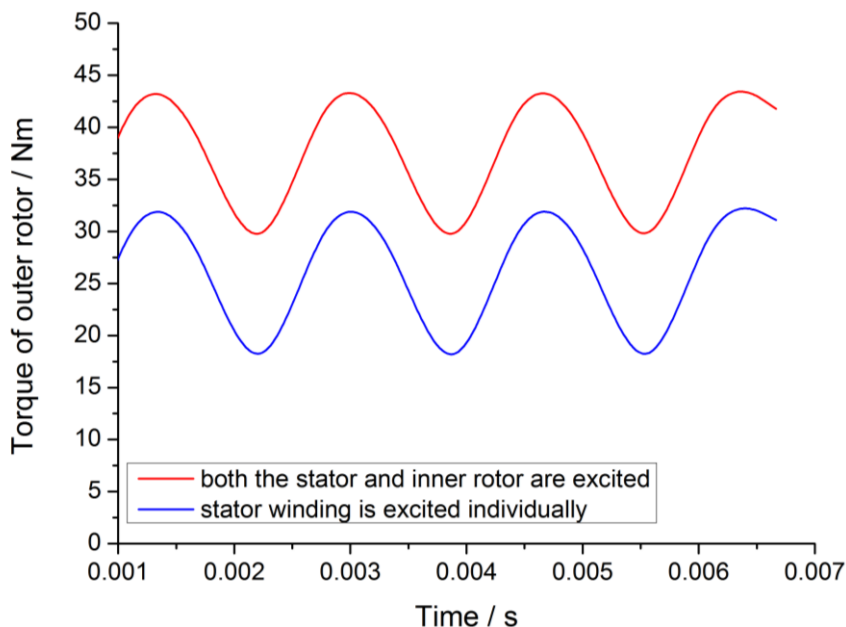


**Figure 22.** The torque waveforms of the inner rotor in different cases.

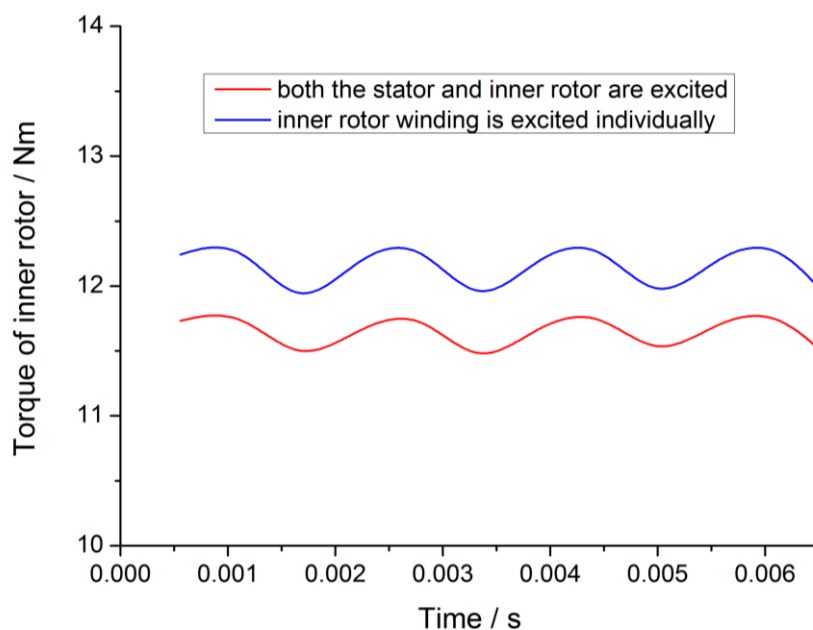
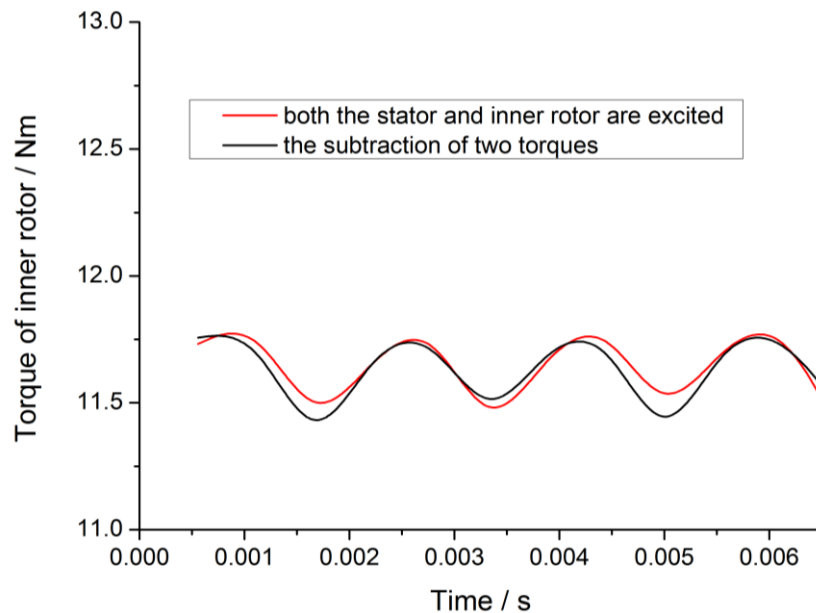


**Figure 23.** The torque waveforms comparison of the inner rotor in different cases.



#### 4. Analysis of Main Parameters' Influence on Performance

Because of the coupling of the magnetic field in the double-rotor machine, FEA method is also utilized to optimize the machine design. In this section, take the main parameters of the outer motor as an example, the influence of the stator and outer rotor pole arc and air gap length for the performance of SRDRM is derived accordingly.

##### 4.1. The Influence of Stator and Rotor Pole Arc on Double-Rotor Machine's Torque

For 4 phase switched reluctance machine, the pole arcs of stator and rotor must guarantee that the rotor possesses the capability of forward and backward self-starting in any case, minimize the minimum inductance per phase when the position is unaligned and minimizes the switching frequency [14]. Therefore, when the stator and rotor of one phase is aligned, the poles of adjacent phase must have some overlap.

$$\begin{cases} \beta_s + \beta_r \leq \frac{2\pi}{N_r} \\ \min(\beta_s, \beta_r) \geq \frac{2\pi}{qN_r} \end{cases} \quad (9)$$

where,  $\beta_s$  is the stator pole arc;  $\beta_r$  is the rotor pole arc;  $q$  is the number of phase; and  $N_r$  is the number of rotor poles.

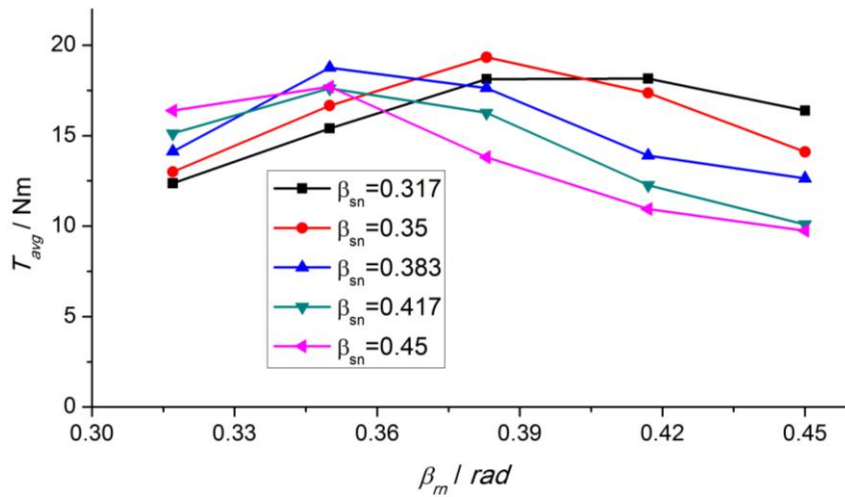
When considering that the influence of the pole arc, because it is related to magnetic field coupling, it is feasible to analyze the double-rotor machine as two separate switched reluctance machines, which significantly simplifies the calculations. In this paper, the outer motor is taken as an example for analysis. The stator and rotor relative pole arcs are defined as:

$$\begin{cases} \beta_{sn} = \beta_s / \tau_r \\ \beta_{rn} = \beta_r / \tau_r \end{cases} \quad (10)$$

where,  $\beta_{sn}$  is the stator relative pole arc;  $\beta_{rm}$  is the rotor relative pole arc; and  $\tau_r$  is the pole pitch of the outer rotor.

The average electromagnetic torque profile of OM with different  $\beta_{sn}$  and  $\beta_{rm}$  are demonstrated in Figure 24.

**Figure 24.** The curves of average electromagnetic torque with different  $\beta_{sn}$  and  $\beta_{rm}$ .



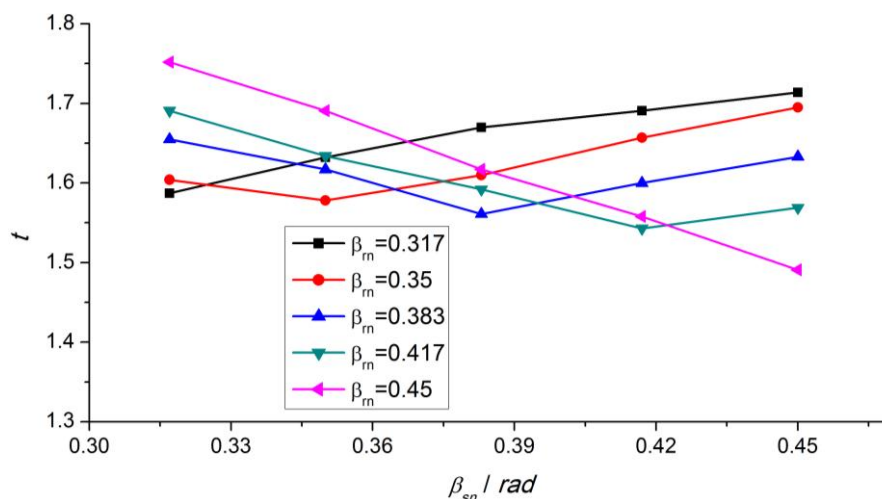
As seen in Figure 24, the average electromagnetic torque approaches the peak value when  $\beta_{sn} = 0.35$  and  $\beta_{rm} = 0.383$ . When  $\beta_{rm} > 0.383$ , the increasing of  $\beta_{sn}$  and  $\beta_{rm}$  will decrease the current and average electromagnetic torque. When  $\beta_{sn} + \beta_{rm} < 0.733$ , the average electromagnetic torque increases with the increasing of  $\beta_{sn}$  and  $\beta_{rm}$ , however, it decreases when  $\beta_{sn} + \beta_{rm} > 0.767$ . Therefore, the stator and rotor pole arcs that maximize the average electromagnetic torque can be chosen in this range.

Figure 25 displays the coefficient of torque ripple with different  $\beta_{sn}$  and  $\beta_{rm}$  at the speed of 1500 rpm. The torque ripple coefficient is obtained by the following formula:

$$t = \frac{T_{max} - T_{min}}{T_{avg}} \tag{11}$$

where,  $T_{max}$ ,  $T_{min}$  and  $T_{avg}$  are the maximum, minimum and average electromagnetic torque respectively.

**Figure 25.** The curves of torque ripple coefficient under different  $\beta_{sn}$  and  $\beta_{rm}$ .



Apparently, the torque ripple coefficient is minimized when  $\beta_{sn} = \beta_{rm}$ , and the torque ripple coefficient decreases with the increase of  $\beta_{sn}$  and  $\beta_{rm}$ .

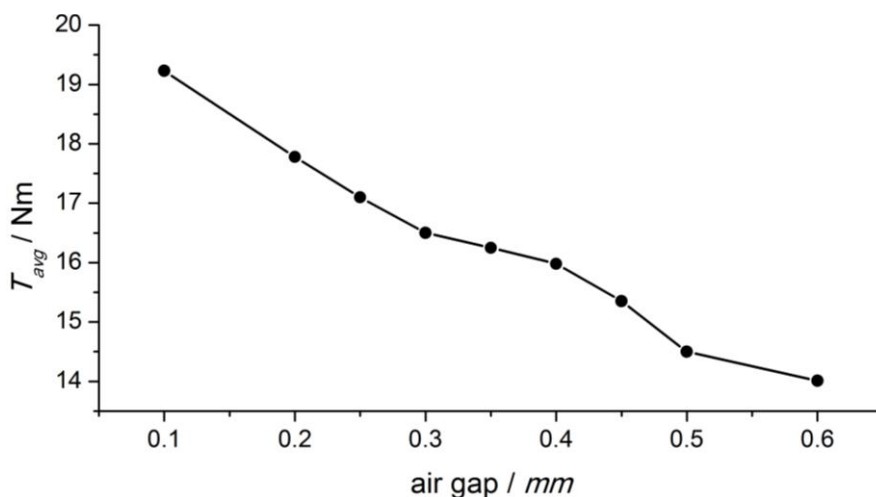
#### 4.2. The Influence of Air Gap on the Torque of Double-Rotor Machine

For switched reluctance machine, the torque is affected by not only the winding current but also the rate of winding inductance change. To get a higher output torque, the winding inductance difference of aligned and unaligned position is expected to be larger, which requires a smaller air gap [15].

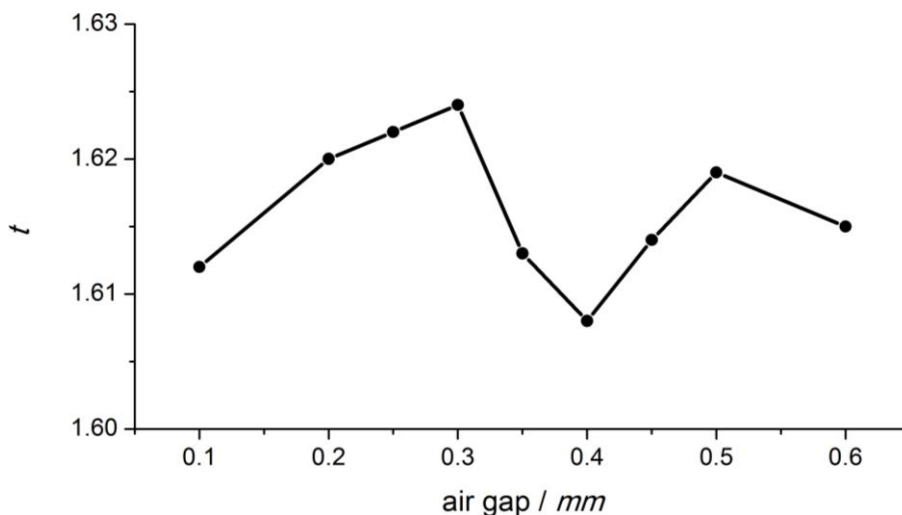
Considering the influence of saturation by the FEA method, the effect of air gap length on the average electromagnetic torque is shown in Figure 26. When the air gap length increases, the aligned inductance decreases significantly, and the torque decreases accordingly. The torque does not vary linearly; the relative flat area varies from 0.35 mm to 0.4 mm.

Figure 27 shows how torque ripple coefficient  $t$  (see Equation (11)) changes with the variation of the air gap. The torque ripple coefficient has a smaller range at a specific value, which is a minimum value when the air gap is 0.4 mm. For the designed prototype machine, it is reasonable if it ranges from 0.35 mm to 0.4 mm. Decreasing or increasing the air gap will increase the torque ripple and lead to vibration and noise.

**Figure 26.** Influence of air gap on average torque.



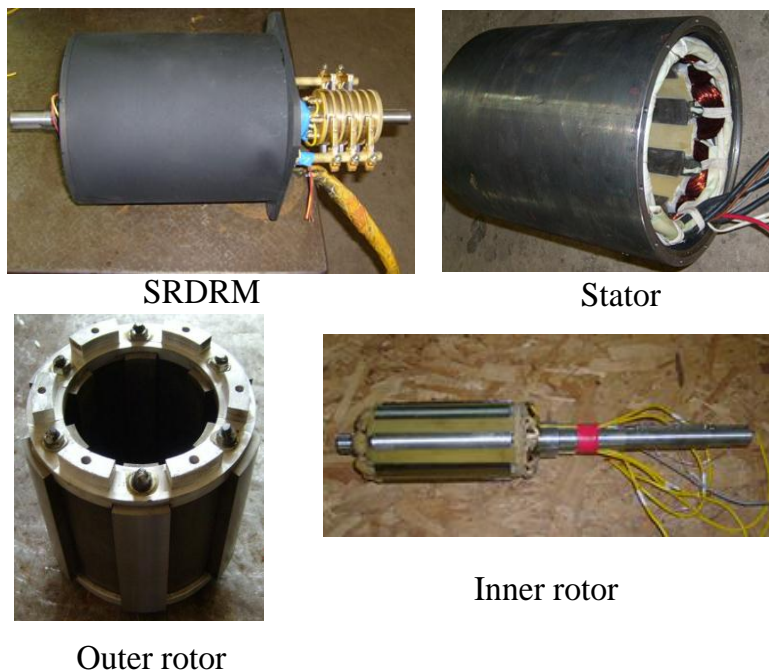
**Figure 27.** Influence of air gap on the torque ripple coefficient.



## 5. Experimental Results

In order to verify the proposed design method, a 4.4 kW SRDRM is designed and manufactured. Figure 28 shows pictures of machine's prototype.

**Figure 28.** Appearance of the prototype and stator/outer rotor/inner rotor.

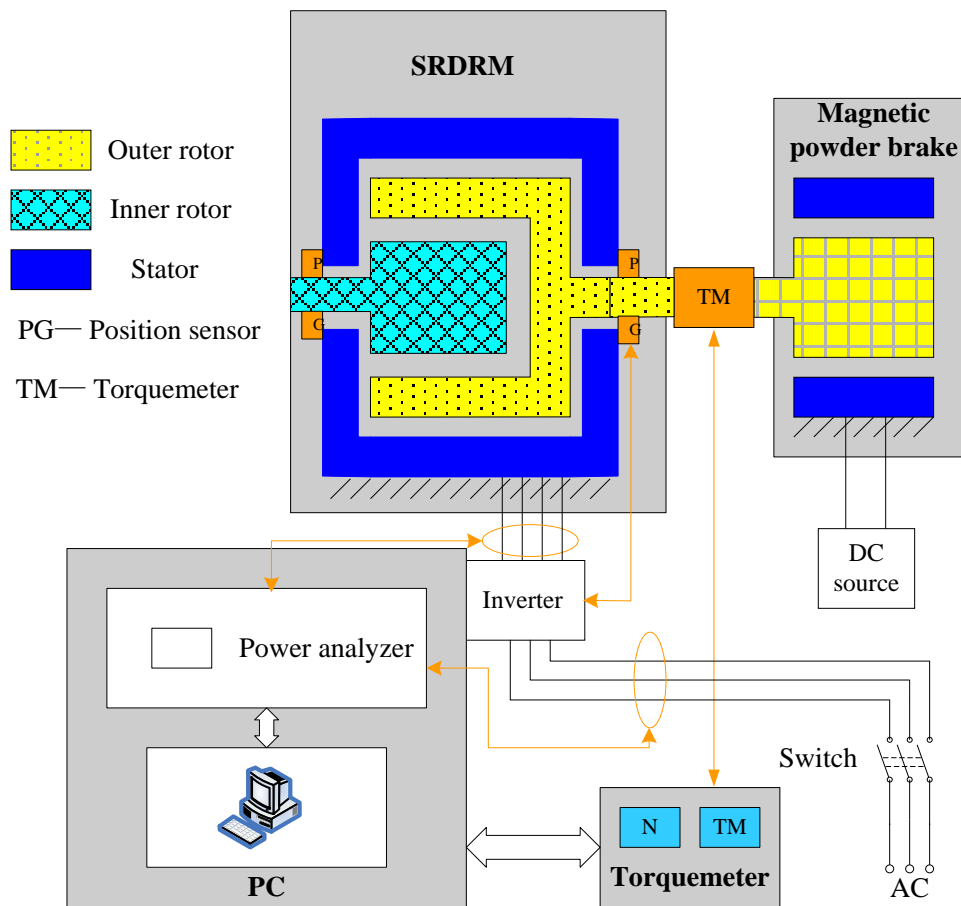


The SRDRM's test bench mainly consists of SRDRM and its controller, magnetic powder brake, torque and speed sensors, power supply, and power meter, showing in Figure 29. Because the limited condition of experiment, only the performance tests of inner motor and outer motor were completed. The focus of future work is the function testing and dynamic control experiment of SRDRM.

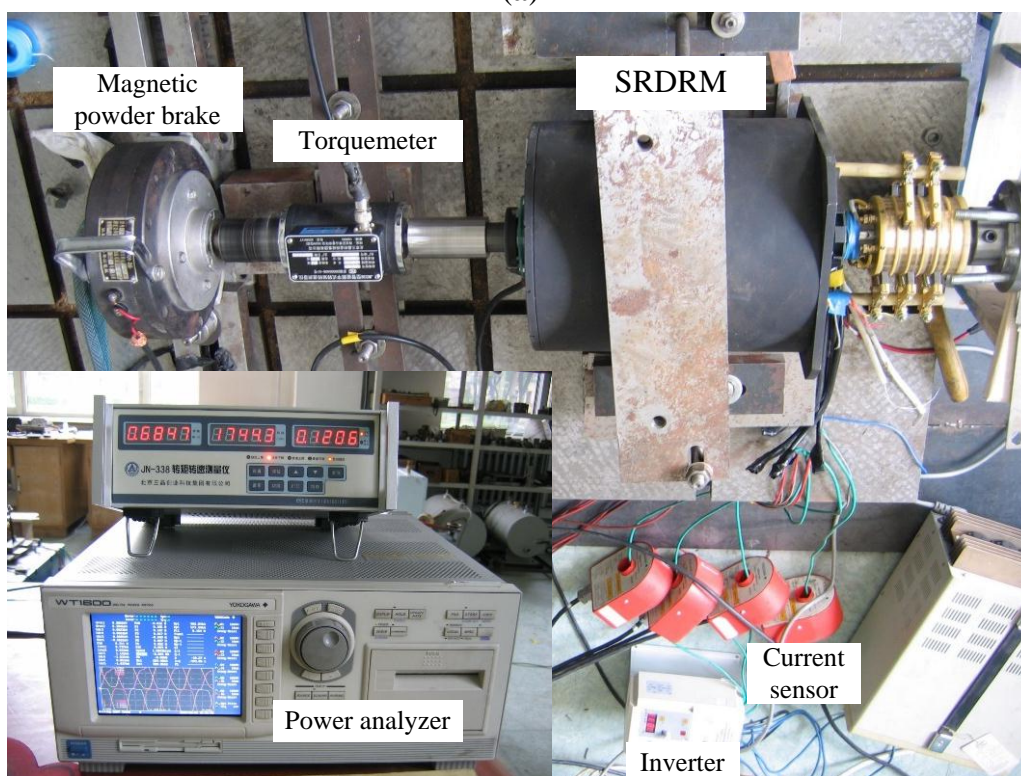
SRDRM's efficiency Map and torque-speed profiles are shown in Figure 30. Figure 30a is the test efficiency Map of outer motor, and the maximum efficiency is 90.4% and the high efficiency region (the area that efficiency >80%) covers 45% of the operational area. Figure 30b is the test efficiency Map of inner motor. Its maximum efficiency is 88.3% and the high efficiency region covers 30% of the operational area. From the experimental results, that the power of outer motor is greater than the designed value, while the power of inner motor is about half of that of the outer motor. Additionally, the maximum efficiency and high efficiency region are both smaller.

As can be seen from the experiment, the IM design is more difficult than the OM. Due to the structure of SRDRM, the effective core volume of IM is much smaller than the OM. Therefore, the inner rotor cannot hold enough conductors, which result in higher thermal load, higher magnetic load, and lower efficiency. Besides, because of the poor heat dissipation condition, the temperature rise in IM will be higher. When designing a SRDRM, in order to get the optimization result, it is better to design the machine from the inside to the outside.

**Figure 29.** The experimental test bench: (a) Schematic diagram of test bench; (b) The experimental test bench.

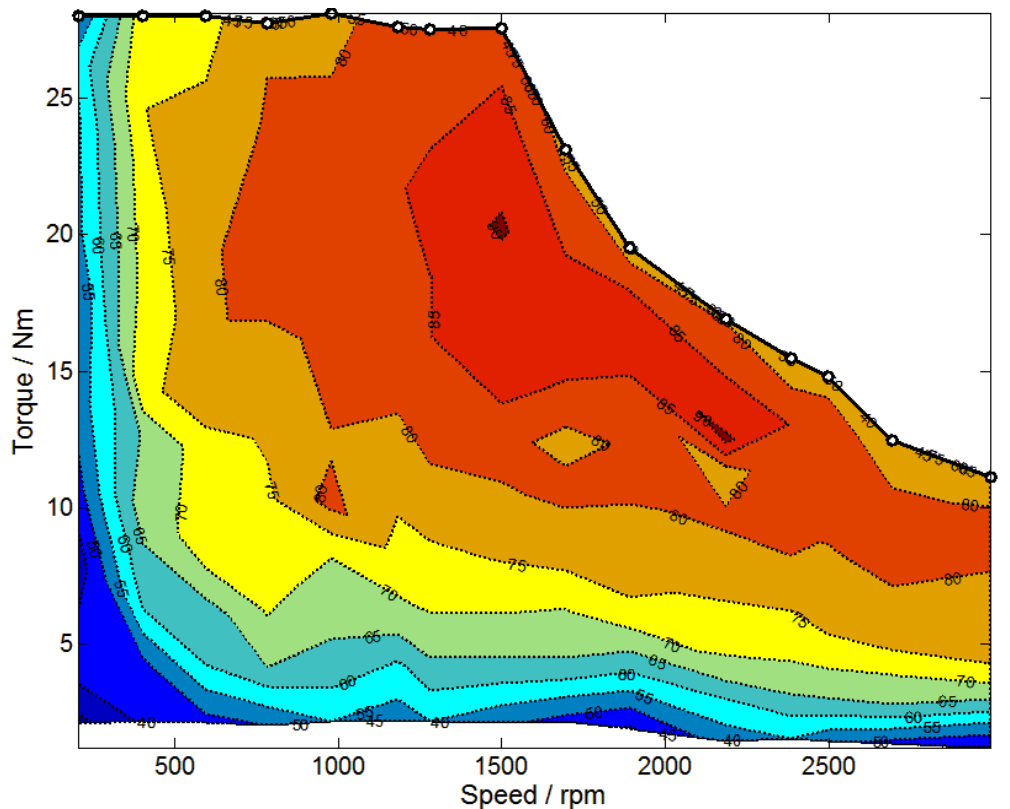


(a)

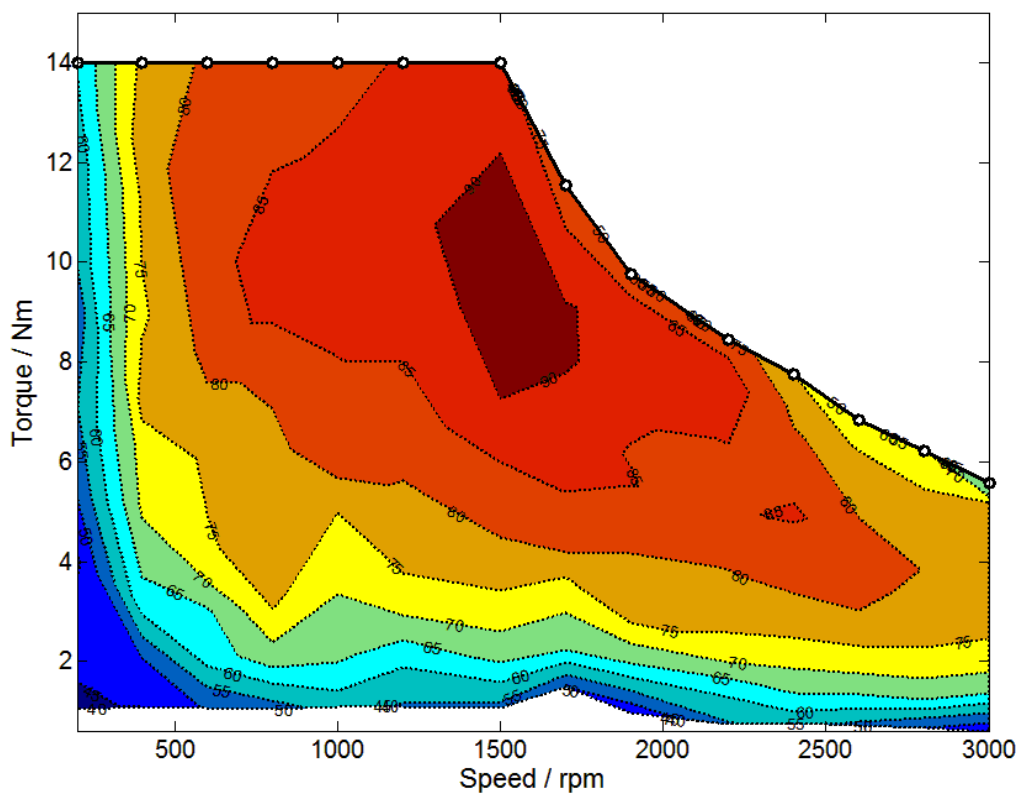


(b)

**Figure 30.** Test efficiency Map of SRDRM: (a) The efficiency Map of outer motor; (b) The efficiency Map of inner motor.



(a)



(b)

## 6. Conclusions

In this paper, a kind of SRDRM for HEVs is studied. Using the magnetic circuit model, the effects of magnet yoke of the outer rotor are analyzed. With the help of 2-D FEA methods, the influence of main parameters, such as pole arc coefficient and air gap on machine performance is analyzed:

1. The SRDRM has a double salient outer rotor, on which there are no conductors or PMs, making it compact and highly reliable. Besides, the constant power speed range is much wider and the cooling problems can be effectively avoided.
2. Outer rotor's magnetic yoke occupies an important position in the electromagnetic design of double-rotor machine. A thinner yoke results in heavy interferences between the fields of stator and inner windings, while a thicker outer rotor yoke will increase the size and weight of the machine.
3. For SRDRM, stator and rotor pole arc, air gap length all have a non-linear effects on average electromagnetic torque and torque ripple and they must be considered comprehensively during the design.
4. IM is smaller and operates in harsh environment. When designing a SRDRM, in order to get the optimized result, the SRDRM should be designed from the inside to the outside.

## Acknowledgments

This research is jointly supported by the National High Technology Research and Development Program of China (863 Program) under Project 2012AA1111003 and the National Natural Science Foundation of China under Project 51277039.

## Author Contributions

Shouliang Han established the finite element model of SRDRM and designed the prototype. Shumei Cui provided many useful suggestions in the construction of paper framework. Liwei Song constructed the experimental platform. This work was conducted under the direction of Ching Chuen Chan. All the authors contributed in different ways during progress of the research work.

## Conflicts of Interest

The authors declare no conflict of interest.

## References

1. Hoeijmakers, M.J.; Ferreira, J.A. The electric variable transmission. *IEEE Trans. Ind. Appl.* **2006**, *42*, 1092–1100.
2. Chau, K.T.; Chan, C.C.; Liu, C. Overview of permanent-magnet brushless drives for electric and hybrid electric vehicles. *IEEE Trans. Ind. Electron.* **2008**, *55*, 2246–2257.
3. Xu, L. Dual-mechanical-port electric machines-concept and application of a new electric. *IEEE Trans. Ind. Appl.* **2009**, *15*, 44–51.

4. Cheng, Y.; Cui, S.; Song, L.; Chan, C.C. The study of the operation modes and control strategies of an advanced electromechanical converter for automobiles. *IEEE Trans. Magn.* **2007**, *43*, 30–433.
5. Zheng, P.; Liu, R.; Thelin, P.; Nordlund, E.; Sadarangani, C. Research on the parameters and performances of a 4QT prototype machine used for HEV. *IEEE Trans. Magn.* **2007**, *43*, 443–446.
6. Zheng, P.; Liu, R.; Wu, Q.; Zhao, J.; Yao, Z. Magnetic coupling analysis of four-quadrant transducer used for hybrid electric vehicles. *IEEE Trans. Magn.* **2007**, *43*, 2597–2599.
7. Zheng, P.; Liu, R.; Thelin, P.; Nordlund, E.; Sadarangani, C. Research on the cooling system of a 4QT prototype machine used for HEV. *IEEE Trans. Energy Convers.* **2008**, *23*, 61–66.
8. Niu, S.; Ho, S.L.; Fu, W.N. A novel double-stator double-rotor brushless electrical continuously variable transmission system. *IEEE Trans. Magn.* **2013**, *49*, 3909–3912.
9. Cui, S.; Yuan, Y.; Wang, T. Research on switched reluctance double-rotor motor used for hybrid electric vehicle. In Proceedings of the International Conference on Electrical Machines and Systems (ICEMS), Wuhan, China, 17–20 October 2008; pp. 3393–3396.
10. Chen Y.; Li, Q.; Zhu, X.; Wei, H.; Zheng, W. Electromagnetic performance analysis of double-rotor stator permanent magnet motor for hybrid electric vehicle. *IEEE Trans. Magn.* **2012**, *48*, 4204–4207.
11. Anekunu, A.Y.; Chowdhury, S.P.; Chowdhury, S. A review of research and development on switched reluctance motor for electric vehicles. In Proceedings of the IEEE Power and Energy Society General Meeting (PES), Vancouver, BC, Canada, 21–25 July 2013; pp. 1–5.
12. Kokernak, J.M.; Torrey, D.A. Magnetic circuit model for the mutually coupled switched reluctance machine. *IEEE Trans. Magn.* **2000**, *36*, 500–507.
13. Sozer, Y.; Torrey, D.A. Optimal turn-off angle control in the face of automatic turn-on angle control for switched-reluctance motors. *IET Electr. Power Appl.* **2007**, *1*, 395–401.
14. Wei, W.; Dunlop, J.B.; Collocott, S.J.; Kalan, B.A. Design optimization of a switched reluctance motor by electromagnetic and thermal finite-element analysis. *IEEE Trans. Magn.* **2003**, *39*, 3334–3336.
15. Kosaka, T.; Kume, A.; Wakayama, H.; Matsui, N. Development of high torque density and efficiency switched reluctance motor with 0.1 mm short airgap. In Proceedings of the IEEE European Conference on Power Electronics and Applications (EPE), Aalborg, Denmark, 2–5 September 2007; pp. 1–9.